HHS Public Access

Author manuscript

Cell Rep. Author manuscript; available in PMC 2017 October 12.

Published in final edited form as:

Cell Rep. 2017 October 10; 21(2): 517–532. doi:10.1016/j.celrep.2017.09.047.

Self-organized cerebral organoids with human specific features predict effective drugs to combat Zika virus infection

Momoko Watanabe[1,2,3], **Jessie E. Buth**[1,2,3], **Neda Vishlaghi**[1,2,3], **Luis de la Torre-Ubieta**[4,5], **Jiannis Taxidis**[5], **Baljit Khakh**[1,6], **Giovanni Coppola**[3,4,5,7], **Caroline A. Pearson**[1,2,3], **Ken Yamauchi**[1,2,3], **Danyang Gong**[8,9], **Xinghong Dai**[8,9], **Robert Damoiseaux**[9], **Roghiyh Aliyari**[10], **Simone Liebscher**[13], **Katja Schenke-Layland**[12,13,14], **Christine Caneda**[3,7], **Eric J. Huang**[15], **Ye Zhang**[3,7], **Genhong Cheng**[10], **Daniel H. Geschwind**[2,3,4,5,11], **Peyman Golshani**[3,4,5,7], **Ren Sun**[8,9], and **Bennett G. Novitch**[1,2,3,16]

[1]Department of Neurobiology, David Geffen School of Medicine at UCLA

[2]Eli and Edythe Broad Center of Regenerative Medicine and Stem Cell Research

[3]Intellectual and Developmental Disabilities Research Center

[4]Center for Autism Research and Treatment and Program in Neurobehavioral Genetics, Semel Institute, David Geffen School of Medicine at UCLA

[5]Department of Neurology, David Geffen School of Medicine at UCLA

[6]Department of Physiology, David Geffen School of Medicine at UCLA

[7]Department of Psychiatry and Biobehavioral Sciences, Semel Institute for Neuroscience and Human Behavior, David Geffen School of Medicine at UCLA

[8]Department of Molecular and Medical Pharmacology

[9]California NanoSystems Institute

[10]Department of Microbiology, Immunology and Molecular Genetics

[11]Department of Human Genetics

[12]Department of Cardiology, David Geffen School of Medicine at UCLA University of California, Los Angeles, Los Angeles, CA 90095, USA

Correspondence to: Bennett G. Novitch.

[16]Lead Contact

Author Contributions: M.W., J.E.B, and N.V. performed all organoid culture experiments and coordinated with others on various analytical procedures. L.T-U., G.C., and D.H.G. performed bioinformatics analyses. J.T., K.Y., and P.G. performed multi-and single photon calcium imaging analyses. C.A.P. and K.Y. contributed materials and imaging analyses. D.G., X.D., and R.S. provided ZIKV samples and help with these experiments. R.D. assisted with automated organoid image analyses. R.A. and G.C. assisted with 25HC studies. S.L., K. S.-L., C.C., E.J.H., Y.Z. provided research materials. M.W., J.E.B., and B.G.N. conceived and designed the experiments with helpful input from the other authors. M.W, J.E.B., and B.G.N. wrote the manuscript.

Accession Numbers: All gene expression data reported in our study have been deposited within the Gene Expression Omnibus (GEO) repository, and are accessible through the GEO Series accession number GSE104279 (www.ncbi.nlm.nih.gov/geo/query/acc.cgi?acc=GSE104279).

[13]Department of Women's Health, Research Institute for Women's Health, Eberhard Karls University Tübingen, 72074 Tübingen, Germany

[14]Department of Cell and Tissue Engineering, Fraunhofer Institute for Interfacial Engineering and Biotechnology, 70569 Stuttgart, Germany

[15]Department of Pathology, University of California, San Francisco, San Francisco, California 94158, USA

Summary

The human cerebral cortex possesses distinct structural and functional features that are not found in the lower species traditionally used to model brain development and disease. Accordingly, considerable attention has been placed on the development of methods to direct pluripotent stem cells to form human brain-like structures termed organoids. However, many organoid differentiation protocols are inefficient and display marked variability in their ability to recapitulate the three-dimensional architecture and course of neurogenesis in the developing human brain. Here, we report optimized organoid culture methods that efficiently and reliably produce cortical and basal ganglia structures similar to those in the human fetal brain in vivo. Neurons within the organoids are functional and exhibit network-like activities. We further demonstrate the utility of this organoid system for modeling the teratogenic effects of Zika virus on the developing brain and identifying more susceptibility receptors and therapeutic compounds that can mitigate its destructive actions.

Graphical abstract

Cerebral organoids recapitulate many aspects of human corticogenesis and are a useful platform for modeling neurodevelopmental mechanisms and diseases. Watanabe et al. describe enhanced organoid methods and model ZIKV pathology. More susceptibility receptors for ZIKV are identified and differential effects of various compounds to mitigate ZIKV-induced cytopathy are demonstrated.

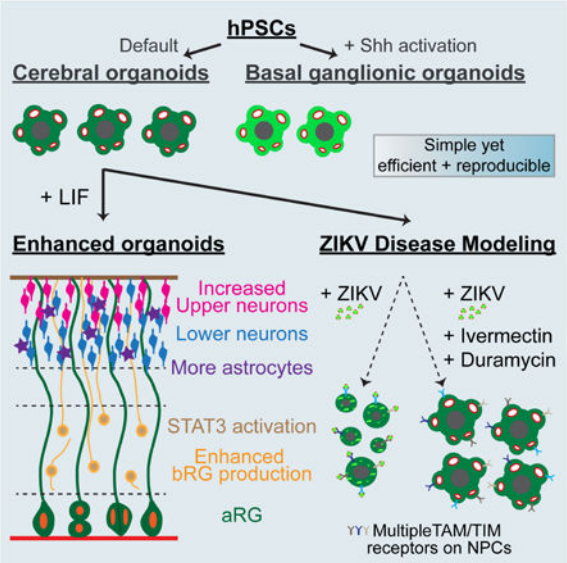

Introduction

The neocortex is a highly conserved region of the central nervous system (CNS) that enables complex sensory activities and higher cognitive functions. It is disproportionately enlarged in humans and other primates (Rakic, 2009), yet the mechanisms underlying its expansion remain poorly defined. The developing neocortex is organized into distinct inner proliferative progenitor compartments, the ventricular zone (VZ) and subventricular zone (SVZ), which give rise to outer neuronal layers in the cortical plate (CP). The VZ and SVZ contain various types of neural progenitors: apical radial glial (aRG) cells in the VZ and basal radial glial (bRG) cells, intermediate progenitors (IPs), and transit amplifying cells in the SVZ. A key contributor to human neocortical growth is an expansion of SVZ progenitors, and defects in this process are thought to underlie a range of neurological disorders (Florio and Huttner, 2014; Sun and Hevner, 2014). The study of early human brain development is challenging due to ethical and practical considerations. Consequently, attention has been placed on the generation of in vitro models using human embryonic and induced pluripotent stem cells (hESC and hIPSC, collectively hPSC).

hPSC have ability to self-renew and differentiate into multiple cell types, and can also self-organize to form three-dimensional (3D) structures with features of tissues in vivo. Initially, CNS development was modeled using adherent radial columnar neuroepithelial cells termed neural rosettes derived from mouse and human ESC (Ying et al., 2003; Zhang et al., 2001). It was later found that PSC-derived cerebral neuroepithelial cells sequentially generate different classes of neurons consistent with corticogenesis in vivo, and exhibit multi-layered organization under certain floating aggregate culture conditions (Eiraku et al., 2008; Gaspard et al., 2008). Recently, several protocols for cerebral organotypic cultures derived from hPSC, often referred to as “organoids” have been established, with improvements in neuronal organization and generation of basal progenitors (Kadoshima et al., 2013; Lancaster et al., 2013; Pasca et al., 2015). Organoid techniques have thus opened the door for studies of human specific developmental features and disease modeling (Bershteyn et al., 2017; Lancaster et al., 2013; Mariani et al., 2015; Qian et al., 2016).

Although cerebral organoid technology is very promising, many challenges remain including rampant batch-to-batch and line-to-line variability and irreproducibility; irregularities in the timing of neuronal maturation, laminar architecture, and cell diversification; unwanted differentiation into other tissue types; and a paucity of direct comparisons of the organoids to native human tissue. Consequently, there is no standardization of the methods used to create cerebral organoids. To realize the potential of organoid systems, it is essential to establish robust and reproducible methods for neural differentiation into specific brain regions to enrich for cells of interest while excluding unwanted cells that confound downstream molecular analyses and applications such as high-throughput phenotypic and therapeutic screening.

Here, we established a simple, yet efficient and reproducible cerebral organoid differentiation method where 80-90% of structures expressed forebrain markers and displayed characteristic neuroepithelial organization. Unbiased transcriptomic analyses confirmed these cerebral organoids closely match fetal brain and developmental transitions

in vivo up to the second trimester. We further found that augmented stimulation of the STAT3 pathway increased the production of basal progenitors, improved the formation and separation of neuronal layers, and promoted astrogliogenesis. Neurons in the cerebral organoids exhibited action potentials and spontaneous ensemble activities. Finally, we used the organoid platform to model Zika virus (ZIKV)-associated microcephaly, identifying additional susceptibility receptors for ZIKV entry into neural progenitors and molecules that can mitigate ZIKV-induced cytopathy. Collectively, our studies provide the community with a reliable and experimentally validated organoid culture system for investigating the mechanistic details underlying human brain development and disease.

Results

Establishment of efficient and reproducible methods for generating cerebral organoids

To initiate organoid formation, we first adapted methods described by Kadoshima et al. 2013 to generate structures from H9 hESC (Figure S1A). Unlike Kadoshima et al. we found that TGFβ, BMP, or WNT inhibitors were not required to facilitate neuronal fate commitment. To enable the long-term survival and growth of the cerebral organoids, cultures were maintained under hyperoxic (40% O2) without the use of mechanical spinners employed in other protocols (Lancaster et al., 2013; Qian et al., 2016). With these parameters, organoids routinely exhibited good structural integrity for over 150 days in culture.

After 2.5 weeks in vitro (W2.5), nearly all aggregates expressed the forebrain markers FOXG1 and LHX2, and general neural progenitor markers such as N-CADHERIN (NCAD), PAX6, and NESTIN (Figures 1A and 1B). Neuroepithelial layers formed on the periphery of the structures with apical-out and basal-in polarity, and an apoptotic region in the middle demarcated by cleaved CASP3 (clCASP3) staining (Figure 1A). Notably, at W2.5 the average size of our cerebral organoids was ~3.15 mm, 2-3 times bigger than those reported using other protocols (Bershteyn et al., 2017; Qian et al., 2016), with marked consistency across nine independent experiments (Figure 1C). Between W2.5 and W5, the neuroepithelial layers exhibited morphogenetic movements that reversed their apicobasal polarity, resulting in uniform neural rosette-like structures within each aggregate (Figure 1A). Similar differentiation results were achieved with other hPSC lines (hESC: UCLA1 and hIPSC: HiPS2 and XFiPS; Figures 1B and S1B-S1C). We also compared the quality and reproducibility of cortical organoids formed with our approach to those achieved using other reported methods (Lancaster and Knoblich, 2014; Lancaster et al., 2013). Our approach appeared more consistent in producing cortical progenitors, and yielded larger and better-organized neuroepithelial rosettes (Figure S2).

We further modified the methods described by Kadoshima et al. by replacing fetal bovine serum in the media at W5 onward with B27 supplement minus Vitamin A. This change increased the numbers of $PAX6^+$ aRG, $TBR2^+$ IP cells, and $CTIP2^+$ neurons, resulting in larger organoids with enhanced laminar organization (Figures 1D-1E, S1A, and S1D). Interestingly, $TBR2^+$ IPs and $PAX6^+$ phosphorylated Vimentin (pVIM+) bRG were disproportionally expanded compared to aRG (Figure S1D, S1G, and S1I-S1J), suggesting that IP and bRG cells are preferentially generated under the B27 media conditions.

Next, we assessed how well the organoids exhibit features of human corticogenesis. At W1, the organoids showed relatively uniform expression of neuroectodermal markers such as SOX2, PAX6, and NCAD with no obvious apicobasal polarity, similar to the profile of neuroepithelial cells in vivo at gestational week 4 (GW4) (Figures S1E-S1F). At W5, cells within the organoid segregated into well-defined $SOX2^+$ VZ progenitor and $TBR1^+$ preplate-like neuronal layers (Figures 1F-1G). By W8, a prominent $TBR2^+$ SVZ, thicker subplate, CP regions, and $REELIN^+$ marginal zone formed, and each compartment continued to expand over time (Figures 1F-1G and S1H). The markers expressed by W8 and older organoids were similarly expressed within the GW14 human fetal cortex (Figures 1H- 1I), indicating that our organoid system efficiently recapitulates the histological organization and patterned expression of key developmental regulators within the human fetal cortex in vivo.

Generation of ventral telencephalic organoids

We examined whether our methods could be modified through the addition of morphogen signals to systematically generate different brain regions. To mimic the ventralizing activities of Sonic hedgehog, which is essential for the formation of the basal ganglionic eminences (GE), we pulsed organoids with Smoothened agonist (SAG) at 15 – 21 days in vitro (Figure S3A). Lateral (LGE), medial (MGE), and caudal (CGE) progenitor markers were upregulated in a SAG dose-dependent manner. Exposure to high amounts of SAG (1 μM) led to the expression of the MGE/CGE marker NKX2.1 in ~50% of cells at W5 (Figures S3B-S3E), followed by broad expression of the GABAergic interneuron marker GAD65 in the neuronal layers of W8 organoids (Figures S3F and S3H). At W10, additional interneuron subtype markers such as SOMATOSTATIN, CALRETININ, and NEUROPEPTIDE Y were expressed, though PARVALBUMIN was undetectable (Figures S3F-S3G). By W14, the neurotransmitter GABA was present in many cells (Figure S3F). Taken together, these results demonstrate that basal GE-like structures and inhibitory interneurons can be readily generated through the addition of ventral patterning signals to our organoid platform.

Transcriptomic analyses confirm that cerebral organoids mimic many features of cortical development in vivo

We next used unbiased bioinformatics analyses (Stein et al., 2014) to examine how closely our cerebral organoids recapitulate human fetal cortex gene expression. In this framework, three core transcriptomic analyses were used: (1) CoNTExT, a machine-learning classifier, to identify the developmental maturity and neuroanatomical identity of individual in vitro samples compared to in vivo specimens, (2) Transition Mapping (TMAP) differential expression analysis to identify which in vitro time points best match in vivo developmental transitions, and (3) weighted gene coexpression network analysis (WGCNA) to identify preserved neurodevelopmental processes.

Hierarchical clustering using the top 5000 most variable genes showed that replicate samples of organoids primarily grouped by developmental stage rather than across time-points (Figure 2A). CoNTExT confirmed their neuroanatomical identity was cortex (Figure 2B) consistent with our immunohistochemical analyses (Figure 1). CoNTExT also indicated that W5 organoids closely match the early embryonic stage of human brain development (period

1, 6-10 GW), whereas W14 organoids match early mid-fetal stages in the second trimester (period 5, 18-21 GW) (Figure 2C).

TMAP was then used to assess how developmental transitions of the organoids matched in vivo. Differential gene expression analyses between pairs of in vivo and in vitro stages were performed, followed by ranking of the resulting gene lists by p-value, and calculation of the significance of the overlap between the gene lists using a hypergeometric test (Figure 2D). We observed strong concordance between W5 vs. W14 organoids and the transition from embryonic to early mid-fetal cortical developmental periods in vivo (periods 1 to 3-4; Figure 2D; max – log10 (p-value) = 545), consistent with the CoNTExT prediction (Figure 2C). We also applied TMAP to compare organoid maturation to the transitions between distinct human fetal cortical laminae in vivo (Figure 2E), which reflect the differentiation of cortical progenitors into neurons and other cell types. The transition between W5 to W14 organoids closely matched the transition between the VZ or SVZ to subplate and cortical plate (Figure 2E). Collectively, these data demonstrate remarkable preservation of gene expression programs between the organoids and the human fetal cortex.

Finally, to determine which specific cellular or biochemical processes are most highly replicated in organoids compared to fetal cortices in vivo, we used WGCNA (Langfelder and Horvath, 2008). WGCNA identified groups of coexpressed genes in prenatal human cortex (Periods 1-8) coupled to module preservation analysis (Langfelder et al., 2011) as implemented in the CoNTExT framework (Stein et al., 2014). Of the 28 modules defined within the human fetal cortex, at least 14 were conserved in cerebral organoids (Figure 2F, Preservation Z score ≥ 4; Table S1) including modules related to neural progenitor mitosis, neurogenesis and gliogenesis, (Modules 4, 3, 5, 15), axon guidance, synaptogenesis, and synaptic transmission (Modules 14, 8, 27, 11, 2, 20), and RNA processing, DNA repair, and ubiquitin proteolysis (Modules 3, 15, 6). By contrast, modules associated with blood vessel development (Module 19) and neuron-microglia interactions (Module 10) were not preserved, consistent with the absence of many non-neural cell populations within the organoids.

STAT3 activation increases human-abundant basal radial glial cells and enhances astrogliogenesis

We next used the organoid system to explore the mechanisms behind the primate-specific abundance of bRG cells. Transcriptional profiling studies for bRG have suggested that elevation of LIFR/STAT3 signaling may contribute to bRG generation in the human cortex (Pollen et al., 2015). bRG cells in the organoids, defined by characteristic markers including SOX2, PAX6, HOPX, ITGβ5, and pVIM, the absence of TBR2, and somatic location within the SVZ, were readily found from W8 onward (Figures 1F-1H, 3A-3D, S1I-S1J, S4A). However, phosphorylation (p, activation) of STAT3 was not apparent (Figure S4A). The addition of recombinant LIF to W5 organoids strongly elevated pSTAT3 staining and led to both a >3-fold increase in bRG cells and thickening of the SVZ by W12 (Figures 3A-3D and S4A-S4C).

Since basal progenitor expansion in the SVZ is implicated in the enlargement of superficial neuronal layers in the human cortex (Rakic, 2009), we examined the organization of the CP

in cerebral organoids after LIF application. Irrespective of LIF inclusion, CTIP2$^+$ or TRB1$^+$ lower layer neurons were distributed throughout the CP. However, with LIF addition SATB2$^+$ and BRN2$^+$ upper layers were enlarged and more clearly segregated outwards in the CP, similar to the distribution of neurons seen in the GW15.5 human fetal CP (Figures 3F and S4D-S4E). LIF application also improved the formation of a LAMININ$^+$ basement membrane at the outer margin of the organoids (Figure 3F). The layered organization of neurons within the organoids persisted up to 22 weeks in culture (the latest time point evaluated), at which time a prominent outer layer of CUX1$^+$ neurons had formed, particularly in the LIF-treated cultures (Figures 3G-3H). Apoptotic cell death was low (Figure 3G), suggesting that these culture conditions are conducive to long-term neuronal survival. Collectively, these results show that LIF application can enhance the production of bRG and formation of defined upper layers of neurons within the organoids.

LIF/STAT3 signaling has also been implicated in promoting astrogliogenesis in the rodent CNS (Fukuda et al., 2007; Nakashima et al., 1999). Without LIF, astrocytes distinguished by GFAP and HepaCAM staining and characteristic star-shaped morphologies were rare in the CP region of W14 organoids (Figure 3E). After LIF addition, GFAP$^+$ astrocytes were readily found along with a smaller number of HepaCAM$^+$ cells (Figures 3E and S5A). We also observed a 30-fold upregulation of GFAP mRNA and increased GFAP protein staining in aRG soma and fibers, most likely reflecting their transition towards astrogliogenesis (Figures 3E and S5A). Regardless of LIF presence or absence, we did not detect signs of oligodendrocyte formation (Figure S4F). Long-term culture of organoids has previously been shown to result in glial overgrowth (Pasca et al., 2015; Renner et al., 2017), but we did not observe this to be the case in the W22 organoids. GFAP$^+$ astrocytes constituted ~8% of the total cell population, less than that found in the human neonatal brain (~40% GFAP+; Figures S5B-S5C).

We lastly compared the astrocyte-promoting effects of LIF to other growth factors known to stimulate the STAT3 pathway including BDNF and GDNF (Ng et al., 2006). BDNF and GDNF did not appear to alter the number of GFAP cells, though we did detect a slight enhancement in HepaCAM staining albeit to a lesser extent than that seen with LIF (Figure S5D). However, the addition of all three factors led to marked upregulation of HepaCAM (Figure S5D), suggesting that their actions can be combined to maximally enhance astrogliogenesis.

Neurons in cerebral organoids are functionally similar to their native counterparts and exhibit spontaneous network activities

To determine the physiological properties of cerebral organoid neurons, we conducted patch clamp recordings within slice preparations. Half of all recorded cells (n = 12 of 24) produced tetrodotoxin-sensitive spike trains upon current stimulation (Figures 4A and 4D). The rectified sodium and potassium currents were then measured in response to current injections. Cells with action potentials (APs) exhibited larger sodium and potassium peak currents compared to those lacking APs (Figures 4B-4D). We also assessed the intrinsic properties of all neurons including membrane potential, membrane resistance, capacitance, peak sodium current, and peak potassium current (Figure 4D and Table S4). The values

recorded in the organoids were strikingly similar to those previously obtained from slices of GW16-22 human fetal cortex (Moore et al., 2009). Only peak amplitudes for sodium and potassium currents were larger in organoids. Together, these data demonstrate that neurons in cerebral organoids have electrophysiological properties that closely match the profiles of neurons recorded from mid-gestational stages of human fetal cortex, consistent with our immunohistochemical, molecular, and bioinformatics analyses.

Next, we examined whether neurons in the organoids exhibit hallmarks of functional maturity and synaptic connectivity. Many CTIP2$^+$ neurons expressed CaMK2α, a kinase associated with calcium signaling and synaptic plasticity, and displayed high levels of SYNAPSIN (SYN) promoter activity driving either Channelrhodopsin2-YFP or the genetically encoded calcium indicator GCaMP6f (Figures 4E-4G′). Punctate staining for the synaptic vesicle associated transporter VGLUT1 was also found at many axosomatic and axodendritic contacts between neurons in 3D reconstructions (Figures 4G-4G′). mRNA expression of additional synaptic markers including SV2A, SYNAPSIN1, and SYNAPTOTAGMIN1, were further confirmed by microarray analyses (Figure S6A).

To test whether cortical neurons in organoids display network functions, structures were infected with SYN::GCaMP6f adeno-associated viruses, and calcium dynamics imaged with resonant scanning two-photon microscopy (Golshani et al., 2009) (Figures 4H and S6B). Many neurons exhibited spontaneous calcium transients typical for action potential spiking (Figure 4H and Movie S1). Firing rates extracted from such events revealed significantly correlated deconvolved calcium transients in ~18% of all neuronal pairs measured (16 pairs out of 14 segmented cells), suggesting partial synchronization (Figures 4I-4J and S6C). Thus, neurons in the cortical organoids appear to exhibit spontaneous ensemble activities.

Cerebral organoids infected with ZIKV display widespread progenitor apoptosis and overall growth restriction

We lastly sought to apply the organoid system towards modeling and ameliorating neurodevelopmental diseases such as microcephaly resulting from ZIKV infection, collectively termed congenital Zika Syndrome (CZS) (Russo et al., 2017). ZIKV envelope protein (E) was readily detected in many cortical cells 3 days post infection (3 dpi) of organoids with a Puerto Rican ZIKV isolate (PRVABC 59), mostly in the VZ and SVZ regions (Figures 5A and S7F). Of the infected cells, 74% were SOX2$^+$ aRG and bRG progenitors, 20% were TBR2$^+$ intermediate progenitors, and 7% were CTIP2$^+$ neurons (Figures 5A and 5D). With respect to each cell type, 75% of the SOX2$^+$ and TBR2$^+$ cells were infected compared to 14% of CTIP2$^+$ neurons (Figure 5D), indicating that ZIKV preferentially infects progenitors.

Previous work has suggested that the susceptibility of neural progenitors to ZIKV infection may be due their expression of the AXL tyrosine kinase receptor, a known entry portal for flaviviruses (Nowakowski et al., 2016). However, more recent studies have found that AXL deletion does not protect these cells from infection (Wells et al., 2016), suggesting the existence of additional entry receptors. Studies in both skin and placental cells have implicated the AXL-related receptor tyrosine kinases TYRO3 and MER (collectively termed TAM receptors), T-cell immunoglobulin and mucin domain (TIM) family receptors, and

CD209 as potential candidates (Hamel et al., 2015; Tabata et al., 2016). In W8 cerebral organoids, AXL, TYRO3, MER, and TIM1 were all prominently localized along the apical surface of aRG cells, with additional punctate staining for TYRO3 and MER seen in both the VZ and SVZ (Figures 5A and 5C). The expression of CD209 was undetectable. We confirmed similar distribution of these receptors in the GW15.5 human fetal cortex (Figures S7B-S7C). Thus, the susceptibility of cortical progenitors to ZIKV is plausibly explained by their prominent expression of at least 4 entry receptors.

We also observed highly infected vesicular structures in the cerebral organoids that were SOX2 and PAX6 negative, yet positive for AXL and the choroid plexus epithelial cell marker AQP1 (Figures 5B and S7A). These findings suggest a potential route of ZIKV entry into the CNS from the bloodstream in vivo given that the highly vascularized choroid plexus secretes cerebral spinal fluid that flows around aRG progenitors, thus exposing them to the virus.

Next, we analyzed the teratogenic effects of ZIKV infection. After 14 dpi, W3 cerebral organoids were stained for HOECHST and propidium iodide (PI) to detect cell death. In mock infected organoids, limited cell death was detected in the necrotic core of the structures (Figure 5E). ZIKV exposure dramatically increased the intensity and extent of PI staining, and reduced the overall size, area, and perimeter of the organoids (Figures 5E-5F). After 14 dpi, 98% of $SOX2^+$ aRG and bRG progenitors, 77% of $TBR2^+$ IPs, and 63% of $CTIP2^+$ neurons were infected with ZIKV (Figures 5G-5H). Apoptotic death was widespread and catastrophic, with 69% of the cells positive for clCASP3 (Figure 5H). The incidence of cell death was similar within each cell type: $SOX2^+$ progenitors 76%, $TBR2^+$ progenitors 72%, and $CTIP2^+$ neurons 69%.

ZIKV infection can also induce spinal cord injury and encephalitis in newborn mice (Fernandes et al., 2017), and has been detected in postmortem human fetal spinal cords (Mlakar et al., 2016). We accordingly tested whether ZIKV could also infect spinal motor neuron progenitors derived from H9 hESC using previously described methods (Adams et al., 2015). After ZIKV exposure, ~80% of cells became infected, followed by widespread apoptotic cell death particularly in $OLIG2^+$ motor neuron progenitors (Figure S7D). $LHX2^+$ cortical progenitors dissociated from cerebral organoids were similarly infected and killed by ZIKV (Figure S7E). These data together show that ZIKV has the capacity to broadly infect and destroy neural progenitors throughout the CNS.

ZIKV infection activates innate immune responses leading to programmed cell death

To better understand how ZIKV affects neural progenitors, we examined the transcriptional changes that precede and coincide with the onset of cell death within infected W8 cortical organoids using RNA sequencing (Figure S8). At 3 dpi, ZIKV E protein was present by immunostaining, but cell death was not seen until 5-7 dpi (Figures 6A-6B). Gene ontology (GO) analyses showed that genes associated with innate immune responses, such as interferon-α, interferon-β, ISG15-protein conjugation, and regulation of viral entry, were all highly upregulated at 3 dpi (Figure 6C and Table S2). On the other hand, genes associated with neural development, differentiation, and morphogenesis were suppressed (Figure 6C and Tables S2-S3), consistent with the decreased expression of neural markers and

reductions in organoid size seen after ZIKV exposure (Figure 5). By 5 dpi, genes associated with the unfolded protein response and apoptotic signaling pathways became highly upregulated, while genes associated with DNA replication, cell cycle progression, and mitosis were downregulated (Figure 6C and Tables S2-S3). Among the 50 genes most upregulated at 3 and 5 dpi, ~28% were implicated with immune system activation and function including several chemokines and cytokines (Table S2). These data support the view that ZIKV can directly and indirectly trigger inflammatory responses leading to neurodegeneration.

Identification of drugs that mitigate the teratogenic effects of ZIKV infection on cortical development

While most of the genes activated by ZIKV infection are known to activate inflammation, ~32% of the induced genes were associated with antiviral activities (Table S2). Of note was Cholesterol 25-Hydroxylase (CH25H), which encodes an enzyme capable of broadly protecting cells from viral infection (Liu et al., 2013). CH25H converts cholesterol to 25-hydroxycholesterol (25HC), a soluble factor that blocks viral entry by inhibiting membrane fusion (Liu et al., 2013). The therapeutic potential for 25HC has been further demonstrated through our recent studies showing that administration to adult non-human primates and mice can reduce viremia and block ZIKV-induced fetal microcephaly when administered during pregnancy (Li et al., 2017). As 25HC is a natural defense protein against several viruses, we tested whether this mechanism could be augmented to alleviate ZIKV-induced cytopathy. Remarkably, addition of 2.5 μM 25HC to the organoid cultures reduced ZIKV mRNA within the organoids by ~74% and the overall number of ZIKV E positive cells by ~72% (Figures 7A, S9A, and S9A′; Table S5). However, there was no appreciable rescue of cell death most likely reflecting mild toxicity seen with sustained exposure of the organoids to 25HC alone (Figure 7A).

Next, we tested whether ZIKV entry and associated pathology could be ameliorated by agents targeting the AXL receptor present on neural progenitors. Organoids were pre-treated with either R428, a small molecule inhibitor of the AXL tyrosine kinase domain (Tabata et al., 2016), or anti-AXL antibodies, both of which have previously been shown to block ZIKV entry and/or spread in some cell types (Hamel et al., 2015; Meertens et al., 2017; Retallack et al., 2016). High levels of R428 had modest effects, reducing ZIKV mRNA levels by ~41%, and clCASP3 staining to a similar extent, though changes in ZIKV E staining were not statistically significant (Figure 7B and Table S5). Anti-AXL antibody treatment was less effective, showing no significant reduction in ZIKV mRNA levels (Figures S9B and S9B′; Table S5). These results are likely explained by the presence of additional viral entry receptors that we have found are highly expressed by neural progenitors in both the organoids and fetal cortex in vivo.

Several studies have reported protective effects of distinct classes of antibiotics in combating flaviviral infection. We tested three candidates, Duramycin, Ivermectin, and Azithromycin. Duramycin is a cyclic peptide approved for veterinary use that is capable of binding to phosphatidylethanolamine residues present in flavivirus virion lipid membrane and thereby blocking their interactions with phosphatidylserine receptors present on target cells

including AXL, TYRO3, MER, and TIM1. Duramycin has shown efficacy in blocking Ebola, Dengue, and West Nile infection in cultured Vero cells (Richard et al., 2015), and recently ZIKV infection of human placental cells (Tabata et al., 2016). Ivermectin and Azithromycin are FDA-approved lipophilic macrolide antibiotics that modulate microbial peptidyltransferases and protein translation. Ivermectin can also bind and inhibit flavivirus helicases needed for viral replication, and block replication of Yellow Fever, West Nile, Dengue, Japanese Encephalitic, and Zika virus in a range of cell lines (Barrows et al., 2016; Mastrangelo et al., 2012). Azithromycin appears capable of reducing ZIKV infection of cultured glial cells (Retallack et al., 2016). Administration of either Duramycin or Ivermectin to the cortical organoids dramatically reduced ZIKV mRNA (76% and 96%, respectively) and both ZIKV E (98% and 97% decrease) and clCASP3 staining (81% and 47% decrease) (Figures 7C-7D and S9D-S9D′; Table S5). While Ivermectin was highly protective against ZIKV infection, its addition alone did lead to a small increase in cell death that was not seen with Duramycin (Figures 7C and 7D; Table S5). By contrast, Azithromycin displayed no significant capacity to reduce ZIKV expression by RT-qPCR or immunostaining (Figures S9C and S9C′; Table S5). Together, these data demonstrate the utility of the cortical organoid system for discriminating between drugs that could mitigate the teratogenic effects of ZIKV infection in the developing human nervous system, and identify Duramycin and Ivermectin as promising leads for further study.

Discussion

Successes and remaining challenges in modeling human brain development in vitro

The ability of hPSC to form 3D brain-like structures allows for the investigation of mechanisms underlying human brain development and disease, but as an emergent technology, technical challenges remain. Here, we established a simple, yet efficient and reproducible cerebral organoid differentiation method that is applicable across hPSC lines, and provide side-by-side comparisons to human fetal cortex using immunohistochemical, transcriptomic, and electrophysiological analyses. We further demonstrate the utility of our organoid platform for modeling the basic mechanisms underlying human corticogenesis and disease.

Thus far, two general approaches have been employed to make organoids: directed differentiation into particular brain regions using defined culture media (Kadoshima et al., 2013; Pasca et al., 2015; Qian et al., 2016) or “whole brain” differentiation methods which permit the spontaneous formation of multiple neural populations (Lancaster et al., 2013). While the latter approach offers the potential to create brain-like structures with more component parts, it comes at the expense of structural consistency, with higher variability between individual organoids and experiments that can confound disease modeling efforts (Quadrato et al., 2016). As no extrinsic factors were used in our differentiation, the nascent neural tissues exhibit a great deal of plasticity, evident by the robust formation of ventral telencephalic structures (MGE/CGE) in response to SHH pathway agonists. GE-organoids offer a means to investigate the mechanisms of interneuron differentiation, migration, and circuit formation.

Since our organoid methods do not require any special apparatus such as spinning bioreactors, the platform is easily scaled up or down. After aggregates are formed in v-shaped 96-well plates, they can be transferred en masse to bacterial dishes or multi-well plates for testing different media conditions or therapeutic compounds. The stationary nature of our system reduces mechanical damage to the organoids, often seen with growth in spinning bioreactors. In the future, further improvement in large-scale production may be achieved by adopting polymer based 3D sphere culture methods (Otsuji et al., 2014).

Expansion of bRG formation and promotion of astrogliogenesis through STAT3 activation

The human cerebral cortex differs from that of lower species, such as rodents, with respect to the expansion of bRG cells and size of the outer SVZ compartment (Florio and Huttner, 2014; Sun and Hevner, 2014). Since bRG are sparse in rodents, human cortical organoids are an ideal model system for investigating the expansion of bRG. It is nevertheless notable that bRG production is modest in many organoid protocols compared to the fetal cortex, suggesting that in vitro culture conditions may not permit the optimal expansion of these cells.

Analyses of the human fetal cortex have suggested that activation of the LIFR/STAT3 pathway may be a characteristic feature of bRG cell maintenance in vivo (Pollen et al., 2015). While expression of LIFR and other bRG markers are preserved in organoids, we found little evidence of STAT3 activation. LIF addition markedly expanded the number of bRG cells and the size of the SVZ, enhanced the separation of neurons into deep and superficial layers, established a basal lamina, and preserved organoid structure and neuronal survival out to W22. LIF also increased the production of astrocytes, consistent with previous reports (Fukuda et al., 2007; Nakashima et al., 1999).

While LIFR/STAT3 signaling is not required for bRG cell formation, it nevertheless appears rate limiting for bRG expansion. The lack of LIF production within the cortical organoids suggests that its origins are other cells that are missing in vitro. Rodent studies have shown that LIF may be maternally supplied and transported to fetal brain tissues through both the vasculature and cerebrospinal fluid (Simamura et al., 2010), and produced locally by the developing choroid plexus (Gregg and Weiss, 2005). Brain endothelial cells secrete LIF and can stimulate astrogliogenesis in culture (Mi et al., 2001), raising the possibility that they could serve a similar function in vivo. Most bRG and IPs reside near blood vessels in the SVZ (Hansen et al., 2010; Stubbs et al., 2009), suggesting an intimate relationship. Together, these findings illustrate both the importance of the interactions of the vasculature and other cell populations within the developing cortex, and the need for fetal tissue research to help discover and explore these connections.

ZIKV-mediated activation of innate immune responses

The recent worldwide outbreak of ZIKV infection and CZS has sparked efforts to understand how the virus causes fetal brain damage and develop means to circumvent. ZIKV can directly infect neural progenitors and disrupt neural development leading to reduced organoid growth and overall size, thus recapitulating microcephaly seen in fetuses and infants exposed to the virus. We also found that ZIKV infection and tissue damage extends

to other regions of the nervous system that we generated from hPSC such as the spinal cord, again modeling some of the neural pathologies seen in patients.

Susceptibility of neural progenitors to infection has been attributed to the expression of AXL (Nowakowski et al., 2016; Retallack et al., 2016), but deletion of AXL from hPSC shows that neural progenitors are still susceptible to ZIKV infection in its absence (Wells et al., 2016). Our studies implicate additional members of the TAM/TIM family of transmembrane receptors, TYRO3, MER, and TIM1, as likely entry portals as their expression was largely confined to VZ and SVZ progenitors along with AXL. Recent studies in mice further indicate that neither single nor combined deletion of two of the three TAM receptors can alleviate ZIKV infection (Hastings et al., 2017), suggesting that expression of even a single receptor may render cells susceptible to the virus.

Insights into how ZIKV triggers cell death have emerged from our and others analysis of transcriptional changes that occur in neural cells after infection (Ghouzzi et al., 2016; Tang et al., 2016; Zhang et al., 2016). Infected cerebral organoids downregulated genes associated with DNA replication, metabolic processes, and cell cycle progression and upregulated DNA damage response genes such as TP53 and those associated with apoptotic cell death. Aberrant activation of DNA-damage repair pathways has been shown to impede neural progenitor expansion and are the root cause of many genetic forms of human microcephaly (Gilmore and Walsh, 2013; O'Driscoll and Jeggo, 2008). Thus, the severe reductions in brain size seen after ZIKV exposure likely reflect both ablation of infected neural progenitors as well as a blockade in their proliferative and neurogenic capacities.

One third of the 50 most upregulated genes following ZIKV infection were associated with interferon signaling and innate immune response preceding the onset of cell death. The extent of these responses may be a primary determinant of neural pathology. Studies comparing neural progenitor death in vitro following exposure to either an African strain of ZIKV, which had not previously been associated with neural damage, or a more recently isolated Asian strain of ZIKV associated with microcephaly, found that the latter elicited a stronger interferon response and TP53 activation, potentially explaining strain-specific pathologies (Zhang et al., 2016). Elevated interferon levels during fetal and postnatal development are also implicated in neuropsychiatric diseases, including schizophrenia, autism, mental retardation, and Down syndrome (Patterson, 2009; Sullivan et al., 2016). Therefore, even though infants exposed to ZIKV might escape structural brain defects, their risk for neurodevelopmental and neuropsychiatric disorders may be significantly elevated. Future studies may provide valuable insights into how aberrant neuroimmune activation impacts the developing brain beyond microcephaly.

Cerebral organoids as models for anti-ZIKV therapies

Currently, there are no approved therapies or vaccines to combat ZIKV infection and its destructive effect on the developing fetal brain. Neural organoids thus provide an invaluable resource to facilitate drug discovery. It is notable that one of the first drugs identified as a potential ZIKV treatment, Azithromycin, can significantly reduce ZIKV infection of cultured glioma cells (Retallack et al., 2016), yet showed little activity in our organoid platform suggesting that its protective effects on the fetal brain may be limited. By contrast,

Ivermectin and Duramycin both displayed marked efficacy in reducing ZIKV infection and neural tissue loss. The potency of Duramycin may reflect its ability to block multiple viral envelope-phosphatidylserine receptor interactions particularly those involving TIM1 (Richard et al., 2015), which we found is prominently expressed by early neural progenitors in vivo along with TAM family members, and faithfully recapitulated in cortical organoids. While the predictive value of the organoid system requires further validation, our studies nonetheless demonstrate its power in singling out therapeutic candidates meriting future investigations.

Experimental Procedures

Pluripotent stem cell culture and organoid differentiation

hPSC experiments were conducted with prior approval from the UCLA Embryonic Stem Cell Research Oversight (ESCRO) Committee. hPSC lines H9, UCLA1, hIPS2 and XFiPS were obtained from the UCLA Broad Stem Cell Research Center Core and maintained on 0.1% gelatin-coated plates with irradiated mouse embryonic feeders in DMEM/F12 (Hyclone) with 20% Knockout Serum Replacement (KSR: Invitrogen), MEM Non-Essential Amino Acids (NEAA: Invitrogen), GlutaMAX (Invitrogen), 0.1 mM β-mercaptoethanol (Invitrogen), 100 μg/ml Primocin (InvivoGen), and 10 ng/ml of FGF2 (Invitrogen). hPSC were maintained at 5% CO2 at 37 °C with daily media change, and were passaged every 6 days at 1:3-1:6 using StemPro EZ Passage tool (Invitrogen). Experiments were performed on cells between passages 40-80 for H9, UCLA1, and hIPS2, and between passages 10-20 for XFiPS.

Cortical organoid differentiation was performed as described (Kadoshima et al., 2013) with several modifications. Briefly, hPSC were dissociated to single cells and plated into low attachment V-bottom 96-well plates (Sumitomo Bakelite, #MS-9096V) to form aggregates in GMEM (Invitrogen), 20% KSR, NEAA, 100 μg/ml Primocin, 0.1 mM β-mercaptoethanol, sodium pyruvate (Invitrogen), and 20 μM ROCK inhibitor (BioPioneer) without Wnt and TGFβ inhibitors. Half of the media was changed every 2-3 days. ROCK inhibitor was removed after 6 days. Aggregates were then transferred to a hyperoxygenated incubator at 5% CO2 and 40% O2 and maintained in DMEM/F12 with N2 (Invitrogen), GlutaMAX, Chemically Defined Lipid Concentrate (CDLC: Invitrogen), and 0.4% methylcellulose (Sigma). Culture media was completely changed every 2-3 days thereafter. On day 35, organoids were cut in half using Vannas spring scissors (Fine Science Tools) and media changed to N2B27 media containing DMEM/F12 supplemented with N2, GlutaMAX, CDLC, 0.4% methylcellulose, B27 without vitamin A (Invitrogen), 1% Growth Factor Reduced Matrigel (Fisher Scientific, #CB-40230), and 5 μg/ml heparin (Sigma). For the FBS method, 10% FBS (Invitrogen) was used in place of B27 without vitamin A. On day 56, organoids were cut in half and transferred to oxygen permeable dishes (Lumox, Sarstedt) containing N2B27 media. Organoids were subsequently cut in half every 2 weeks and routinely sustained for up to 150 days. For STAT3 activation, Leukemia Inhibitory Factor (LIF, Millipore) was added at 2,000 U/mL from D35 onward. At the end of the experiments, organoids were processed for immunohistochemical and RNA analyses as described in the

Supplemental Experimental Procedures. See Table S6 for key resources and Table S7 for antibody information.

ZIKV Infection

Zika virus strain PRVABC59 was obtained from the United States Centers for Disease Control and Prevention (CDC) and further amplified in *Aedes albopictus* C6/36 cells. Briefly, C6/36 cells were infected at a MOI of 0.05 for 10 days. Cell culture supernatant was collected, centrifuged at 8,000 × g for 10 minutes at 4°C, and frozen in aliquots at -80°C. Supernatants from uninfected C3/36 cells were collected as control media for mock infection. Viral titer was determined to be about 10^7 PFU/ml by standard plaque assay on Vero cells.

For infection, each organoid (~80,000 cells/W3 organoid, ~150,000 cells/W8 organoid) was inoculated with 1:2-1:8 viral stocks diluted in N2 based media (MOI ~0.3 to 3.125, see Figure S7F) as previously described (Li et al., 2017) and incubated for 2 hours. Thereafter, viral stocks were further diluted 1:2 with fresh culture media. Organoids were maintained with the diluted virus for 24 hours, and then media containing ZIKV was removed and replaced with fresh culture media. Media was then changed every 2-3 days for the remainder of the experiment. Organoids were collected and analyzed by RT-qPCR and immunohistochemistry at various time points. Details for the administration of anti-ZIKV drugs are described in the Supplemental Experimental Procedures.

Supplementary Material

Refer to Web version on PubMed Central for supplementary material.

Acknowledgments

We are grateful to B. Van Handel, K. Morizono, and the Broad Stem Cell Research Center (BSCRC) Stem Cell Core for materials, D. Moore and D. Sivalingam for technical assistance, the UCLA Clinical Microarray Core and F. Gao (Informatics Center for Neurogenetics and Neurogenomics) for assistance with RNA sequencing experiments and data analysis, and the Molecular Screening Shared Resource and BSCRC microscopy core for access to imaging facilities. We also thank S. Butler, W. Lowry, and D. Silver for invaluable discussions and comments on the manuscript. M.W. is very thankful to Y. Sasai for mentorship, and H. Sakaguchi and T. Kadoshima for invaluable technical and intellectual interactions. This work was supported by research awards from the UCLA Eli and Edythe Broad Center of Regenerative Medicine and Stem Cell Research, the Rose Hills Foundation, The Binder Family Foundation, the UCLA Clinical and Translational Science Institute, and grants from the California Institute for Regenerative Medicine (CIRM) (DISC1-08819) and the National Institute of Health (NIH) (R01NS089817l, R01NS085227) to B.G.N.; M.W. was supported by postdoctoral training awards provided by the UCLA Broad Stem Cell Research Center and the Uehara Memorial Foundation; J.E.B. and N.V. were supported in part by the UCLA-California State University Northridge CIRM-Bridges training program (TB1-00183), D.H.G. was supported by NIH grants R01MH060233, R01MH100027, U01MH103339, R01MH110927, and R01MH094714); L.T.U was supported by the California Institute for Regenerative Medicine (CIRM)-BSCRC Training Grant (TG2-01169); G.C. was supported by NIH grants R01AI069120, R01AI056154, and R01AI078389); Y.Z. was supported by NIH grant R00NS089780; E.H. was (supported by NIH grant P01NS083513; S.L. and K.S.-L. were supported by the Ministry of Science, Research and Arts of Baden-Württemberg (Az.: 33-729.55-3/214). We also acknowledge the support of the NINDS Informatics Center for Neurogenetics and Neurogenomics P30NS062691 to G.C.) and both the Cells, Circuits and Systems Analysis and Genetics and Genomics Cores of the Semel Institute of Neuroscience at UCLA, which are supported by the NICHD (U54HD087101).

References

Adams KL, Rousso DL, Umbach JA, Novitch BG. Foxp1-mediated programming of limb-innervating motor neurons from mouse and human embryonic stem cells. Nat Commun. 2015; 6:6778. [PubMed: 25868900]

Barrows NJ, Campos RK, Powell ST, Prasanth KR, Schott-Lerner G, Soto-Acosta R, Galarza-Munoz G, McGrath EL, Urrabaz-Garza R, Gao J, et al. A Screen of FDA-Approved Drugs for Inhibitors of Zika Virus Infection. Cell Host Microbe. 2016; 20:259–270. [PubMed: 27476412]

Bershteyn M, Nowakowski TJ, Pollen AA, Di Lullo E, Nene A, Wynshaw-Boris A, Kriegstein AR. Human iPSC-Derived Cerebral Organoids Model Cellular Features of Lissencephaly and Reveal Prolonged Mitosis of Outer Radial Glia. Cell Stem Cell. 2017

Eiraku M, Watanabe K, Matsuo-Takasaki M, Kawada M, Yonemura S, Matsumura M, Wataya T, Nishiyama A, Muguruma K, Sasai Y. Self-organized formation of polarized cortical tissues from ESCs and its active manipulation by extrinsic signals. Cell Stem Cell. 2008; 3:519–532. [PubMed: 18983967]

Fernandes NC, Nogueira JS, Ressio RA, Cirqueira CS, Kimura LM, Fernandes KR, Cunha MS, Souza RP, Guerra JM. Experimental Zika virus infection induces spinal cord injury and encephalitis in newborn Swiss mice. Exp Toxicol Pathol. 2017; 69:63–71. [PubMed: 27899230]

Florio M, Huttner WB. Neural progenitors, neurogenesis and the evolution of the neocortex. Development. 2014; 141:2182–2194. [PubMed: 24866113]

Fukuda S, Abematsu M, Mori H, Yanagisawa M, Kagawa T, Nakashima K, Yoshimura A, Taga T. Potentiation of astrogliogenesis by STAT3-mediated activation of bone morphogenetic protein-Smad signaling in neural stem cells. Mol Cell Biol. 2007; 27:4931–4937. [PubMed: 17452461]

Gaspard N, Bouschet T, Hourez R, Dimidschstein J, Naeije G, van den Ameele J, Espuny-Camacho I, Herpoel A, Passante L, Schiffmann SN, et al. An intrinsic mechanism of corticogenesis from embryonic stem cells. Nature. 2008; 455:351–357. [PubMed: 18716623]

Ghouzzi VE, Bianchi FT, Molineris I, Mounce BC, Berto GE, Rak M, Lebon S, Aubry L, Tocco C, Gai M, et al. ZIKA virus elicits P53 activation and genotoxic stress in human neural progenitors similar to mutations involved in severe forms of genetic microcephaly and p53. Cell Death Dis. 2016; 7:e2440. [PubMed: 27787521]

Gilmore EC, Walsh CA. Genetic causes of microcephaly and lessons for neuronal development. Wiley Interdiscip Rev Dev Biol. 2013; 2:461–478. [PubMed: 24014418]

Golshani P, Goncalves JT, Khoshkhoo S, Mostany R, Smirnakis S, Portera-Cailliau C. Internally mediated developmental desynchronization of neocortical network activity. J Neurosci. 2009; 29:10890–10899. [PubMed: 19726647]

Gregg C, Weiss S. CNTF/LIF/gp130 receptor complex signaling maintains a VZ precursor differentiation gradient in the developing ventral forebrain. Development. 2005; 132:565–578. [PubMed: 15634701]

Hamel R, Dejarnac O, Wichit S, Ekchariyawat P, Neyret A, Luplertlop N, Perera-Lecoin M, Surasombatpattana P, Talignani L, Thomas F, et al. Biology of Zika Virus Infection in Human Skin Cells. J Virol. 2015; 89:8880–8896. [PubMed: 26085147]

Hansen DV, Lui JH, Parker PR, Kriegstein AR. Neurogenic radial glia in the outer subventricular zone of human neocortex. Nature. 2010; 464:554–561. [PubMed: 20154730]

Hastings AK, Yockey LJ, Jagger BW, Hwang J, Uraki R, Gaitsch HF, Parnell LA, Cao B, Mysorekar IU, Rothlin CV, et al. TAM Receptors Are Not Required for Zika Virus Infection in Mice. Cell Rep. 2017; 19:558–568. [PubMed: 28423319]

Kadoshima T, Sakaguchi H, Nakano T, Soen M, Ando S, Eiraku M, Sasai Y. Self-organization of axial polarity, inside-out layer pattern, and species-specific progenitor dynamics in human ES cell-derived neocortex. Proc Natl Acad Sci U S A. 2013; 110:20284–20289. [PubMed: 24277810]

Lancaster MA, Knoblich JA. Generation of cerebral organoids from human pluripotent stem cells. Nat Protoc. 2014; 9:2329–2340. [PubMed: 25188634]

Lancaster MA, Renner M, Martin CA, Wenzel D, Bicknell LS, Hurles ME, Homfray T, Penninger JM, Jackson AP, Knoblich JA. Cerebral organoids model human brain development and microcephaly. Nature. 2013; 501:373–379. [PubMed: 23995685]

Langfelder P, Horvath S. WGCNA: an R package for weighted correlation network analysis. BMC Bioinformatics. 2008; 9:559. [PubMed: 19114008]

Langfelder P, Luo R, Oldham MC, Horvath S. Is my network module preserved and reproducible? PLoS Comput Biol. 2011; 7:e1001057. [PubMed: 21283776]

Li C, Deng YQ, Wang S, Ma F, Aliyari R, Huang XY, Zhang NN, Watanabe M, Dong HL, Liu P, et al. 25-Hydroxycholesterol Protects Host against Zika Virus Infection and Its Associated Microcephaly in a Mouse Model. Immunity. 2017; 46:446–456. [PubMed: 28314593]

Liu SY, Aliyari R, Chikere K, Li G, Marsden MD, Smith JK, Pernet O, Guo H, Nusbaum R, Zack JA, et al. Interferon-inducible cholesterol-25-hydroxylase broadly inhibits viral entry by production of 25-hydroxycholesterol. Immunity. 2013; 38:92–105. [PubMed: 23273844]

Mariani J, Coppola G, Zhang P, Abyzov A, Provini L, Tomasini L, Amenduni M, Szekely A, Palejev D, Wilson M, et al. FOXG1-Dependent Dysregulation of GABA/Glutamate Neuron Differentiation in Autism Spectrum Disorders. Cell. 2015; 162:375–390. [PubMed: 26186191]

Mastrangelo E, Pezzullo M, De Burghgraeve T, Kaptein S, Pastorino B, Dallmeier K, de Lamballerie X, Neyts J, Hanson AM, Frick DN, et al. Ivermectin is a potent inhibitor of flavivirus replication specifically targeting NS3 helicase activity: new prospects for an old drug. J Antimicrob Chemother. 2012; 67:1884–1894. [PubMed: 22535622]

Meertens L, Labeau A, Dejarnac O, Cipriani S, Sinigaglia L, Bonnet-Madin L, Le Charpentier T, Hafirassou ML, Zamborlini A, Cao-Lormeau VM, et al. Axl Mediates ZIKA Virus Entry in Human Glial Cells and Modulates Innate Immune Responses. Cell Rep. 2017; 18:324–333. [PubMed: 28076778]

Mi H, Haeberle H, Barres BA. Induction of astrocyte differentiation by endothelial cells. J Neurosci. 2001; 21:1538–1547. [PubMed: 11222644]

Mlakar J, Korva M, Tul N, Popovic M, Poljsak-Prijatelj M, Mraz J, Kolenc M, Resman Rus K, Vesnaver Vipotnik T, Fabjan Vodusek V, et al. Zika Virus Associated with Microcephaly. N Engl J Med. 2016; 374:951–958. [PubMed: 26862926]

Moore AR, Filipovic R, Mo Z, Rasband MN, Zecevic N, Antic SD. Electrical excitability of early neurons in the human cerebral cortex during the second trimester of gestation. Cereb Cortex. 2009; 19:1795–1805. [PubMed: 19015375]

Nakashima K, Yanagisawa M, Arakawa H, Kimura N, Hisatsune T, Kawabata M, Miyazono K, Taga T. Synergistic signaling in fetal brain by STAT3-Smad1 complex bridged by p300. Science. 1999; 284:479–482. [PubMed: 10205054]

Ng YP, Cheung ZH, Ip NY. STAT3 as a downstream mediator of Trk signaling and functions. J Biol Chem. 2006; 281:15636–15644. [PubMed: 16611639]

Nowakowski TJ, Pollen AA, Di Lullo E, Sandoval-Espinosa C, Bershteyn M, Kriegstein AR. Expression Analysis Highlights AXL as a Candidate Zika Virus Entry Receptor in Neural Stem Cells. Cell Stem Cell. 2016; 18:591–596. [PubMed: 27038591]

O'Driscoll M, Jeggo PA. The role of the DNA damage response pathways in brain development and microcephaly: insight from human disorders. DNA Repair (Amst). 2008; 7:1039–1050. [PubMed: 18458003]

Otsuji TG, Bin J, Yoshimura A, Tomura M, Tateyama D, Minami I, Yoshikawa Y, Aiba K, Heuser JE, Nishino T, et al. A 3D sphere culture system containing functional polymers for large-scale human pluripotent stem cell production. Stem Cell Reports. 2014; 2:734–745. [PubMed: 24936458]

Pasca AM, Sloan SA, Clarke LE, Tian Y, Makinson CD, Huber N, Kim CH, Park JY, O'Rourke NA, Nguyen KD, et al. Functional cortical neurons and astrocytes from human pluripotent stem cells in 3D culture. Nat Methods. 2015; 12:671–678. [PubMed: 26005811]

Patterson PH. Immune involvement in schizophrenia and autism: etiology, pathology and animal models. Behav Brain Res. 2009; 204:313–321. [PubMed: 19136031]

Pollen AA, Nowakowski TJ, Chen J, Retallack H, Sandoval-Espinosa C, Nicholas CR, Shuga J, Liu SJ, Oldham MC, Diaz A, et al. Molecular identity of human outer radial glia during cortical development. Cell. 2015; 163:55–67. [PubMed: 26406371]

Qian XY, Nguyen HN, Song MM, Hadiono C, Ogden SC, Hammack C, Yao B, Hamersky GR, Jacob F, Zhong C, et al. Brain-Region-Specific Organoids Using Mini-bioreactors for Modeling ZIKV Exposure. Cell. 2016; 165:1238–1254. [PubMed: 27118425]

Quadrato G, Brown J, Arlotta P. The promises and challenges of human brain organoids as models of neuropsychiatric disease. Nat Med. 2016; 22:1220–1228. [PubMed: 27783065]

Rakic P. Evolution of the neocortex: a perspective from developmental biology. Nat Rev Neurosci. 2009; 10:724–735. [PubMed: 19763105]

Renner M, Lancaster MA, Bian S, Choi H, Ku T, Peer A, Chung K, Knoblich JA. Self-organized developmental patterning and differentiation in cerebral organoids. EMBO J. 2017; 36:1316–1329. [PubMed: 28283582]

Retallack H, Di Lullo E, Arias C, Knopp KA, Laurie MT, Sandoval-Espinosa C, Mancia Leon WR, Krencik R, Ullian EM, Spatazza J, et al. Zika virus cell tropism in the developing human brain and inhibition by azithromycin. Proc Natl Acad Sci U S A. 2016; 113:14408–14413. [PubMed: 27911847]

Richard AS, Zhang A, Park SJ, Farzan M, Zong M, Choe H. Virion-associated phosphatidylethanolamine promotes TIM1-mediated infection by Ebola, dengue, and West Nile viruses. Proc Natl Acad Sci U S A. 2015; 112:14682–14687. [PubMed: 26575624]

Russo FB, Jungmann P, Beltrao-Braga PCB. Zika infection and the development of neurological defects. Cell Microbiol. 2017; 19

Simamura E, Shimada H, Higashi N, Uchishiba M, Otani H, Hatta T. Maternal leukemia inhibitory factor (LIF) promotes fetal neurogenesis via a LIF-ACTH-LIF signaling relay pathway. Endocrinology. 2010; 151:1853–1862. [PubMed: 20160138]

Stein JL, de la Torre-Ubieta L, Tian Y, Parikshak NN, Hernandez IA, Marchetto MC, Baker DK, Lu D, Hinman CR, Lowe JK, et al. A quantitative framework to evaluate modeling of cortical development by neural stem cells. Neuron. 2014; 83:69–86. [PubMed: 24991955]

Stubbs D, DeProto J, Nie K, Englund C, Mahmud I, Hevner R, Molnar Z. Neurovascular congruence during cerebral cortical development. Cereb Cortex. 2009; 19 Suppl 1:i32–41. [PubMed: 19386634]

Sullivan KD, Lewis HC, Hill AA, Pandey A, Jackson LP, Cabral JM, Smith KP, Liggett LA, Gomez EB, Galbraith MD, et al. Trisomy 21 consistently activates the interferon response. Elife. 2016; 5:e16220. [PubMed: 27472900]

Sun T, Hevner RF. Growth and folding of the mammalian cerebral cortex: from molecules to malformations. Nat Rev Neurosci. 2014; 15:217–232. [PubMed: 24646670]

Tabata T, Petitt M, Puerta-Guardo H, Michlmayr D, Wang C, Fang-Hoover J, Harris E, Pereira L. Zika Virus Targets Different Primary Human Placental Cells, Suggesting Two Routes for Vertical Transmission. Cell Host Microbe. 2016; 20:155–166. [PubMed: 27443522]

Tang H, Hammack C, Ogden SC, Wen Z, Qian X, Li Y, Yao B, Shin J, Zhang F, Lee EM, et al. Zika Virus Infects Human Cortical Neural Progenitors and Attenuates Their Growth. Cell Stem Cell. 2016; 18:587–590. [PubMed: 26952870]

Wells MF, Salick MR, Wiskow O, Ho DJ, Worringer KA, Ihry RJ, Kommineni S, Bilican B, Klim JR, Hill EJ. Genetic ablation of AXL does not protect human neural progenitor cells and cerebral organoids from Zika virus infection. Cell Stem Cell. 2016; 19:703–708. [PubMed: 27912091]

Ying QL, Stavridis M, Griffiths D, Li M, Smith A. Conversion of embryonic stem cells into neuroectodermal precursors in adherent monoculture. Nat Biotechnol. 2003; 21:183–186. [PubMed: 12524553]

Zhang F, Hammack C, Ogden SC, Cheng Y, Lee EM, Wen Z, Qian X, Nguyen HN, Li Y, Yao B, et al. Molecular signatures associated with ZIKV exposure in human cortical neural progenitors. Nucleic Acids Res. 2016; 44:8610–8620. [PubMed: 27580721]

Zhang SC, Wernig M, Duncan ID, Brustle O, Thomson JA. In vitro differentiation of transplantable neural precursors from human embryonic stem cells. Nat Biotechnol. 2001; 19:1129–1133. [PubMed: 11731781]

Highlights

- Simple yet efficient and reproducible methods for generating human brain organoids

- STAT3 signaling increases bRG cell formation, corticogenesis, and astrogliogenesis

- Identification of TIM1, TYRO3, & MER as candidate ZIKV receptors in the fetal brain

- Identification of multiple compounds capable of mitigating ZIKV-induced cytopathy

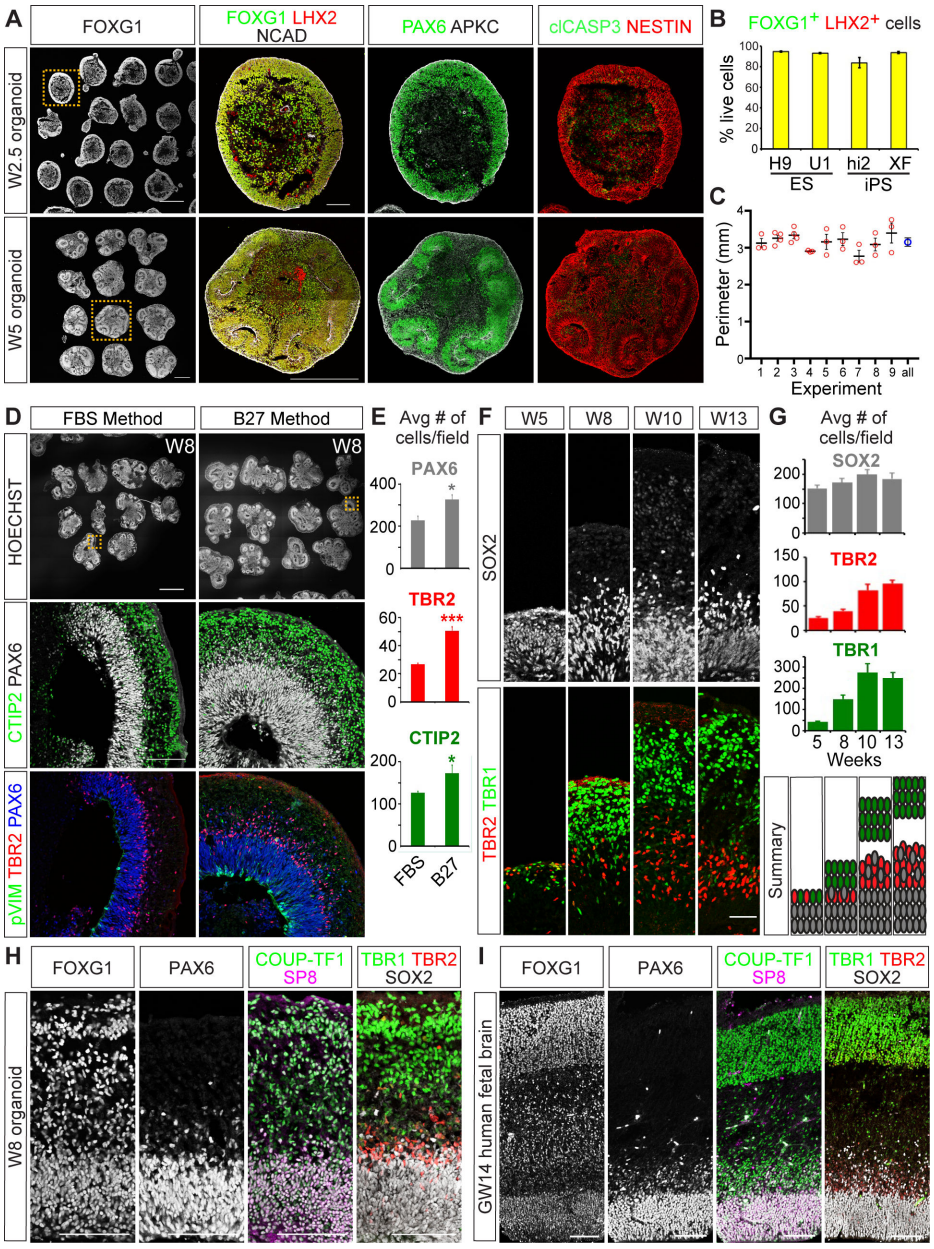

Figure 1. Establishment of highly reproducible cortical organoid methods that recapitulate human development in vivo

(**A**) Cerebral organoids immunostained for telencephalic (FOXG1/LHX2/PAX6), apical membrane (NCAD/APKC), progenitor (NESTIN), and cell death (clCASP3) markers. (**B**) Percentage of FOXG1^{+} and LHX2^{+} cells out of total live cells per organoid. hESC lines, H9 and UCLA1 (U1), and hIPSC lines, HiPS2 (Hi2) and XFiPS (XF). H9 n = 9, n = 3 for other lines. Data are represented as mean ± SEM. (**C**) The perimeters of W2.5 organoids derived from H9 across nine experiments plotted as mean ± SEM. All (blue circle) indicates the summation of all samples plotted as mean and 95% confidence intervals. No significance between samples by one-way ANOVA. (**D-E**) Comparison of FBS versus B27 media components, showing CTIP2^{+} neurons, TBR2^{+} intermediate progenitor, PAX6^{+} progenitor,

and pVIM^{+} dividing RG cell markers n=3. Data are represented as mean ± SEM. (**F**) Laminar growth of cerebral organoids showing SOX2^{+} progenitor, TBR2^{+} intermediate progenitor, and TBR1^{+} neurons. (**G**) Average number of cells per field ± SEM at various time points. n=3. (H-I) Comparative immunohistochemical analyses of W8 cerebral organoids (**H**) and GW14 human fetal cortex (**I**). Scale bars: A FOXG1 and W5 FOXG1/LHX2/NCAD 500 μm; A W2.5 FOXG1/LHX2/NCAD, D, H, I, 100 μm; D HOESCHT, 1mm; F, 50 μm. See also Figures S1, S2, and S3.

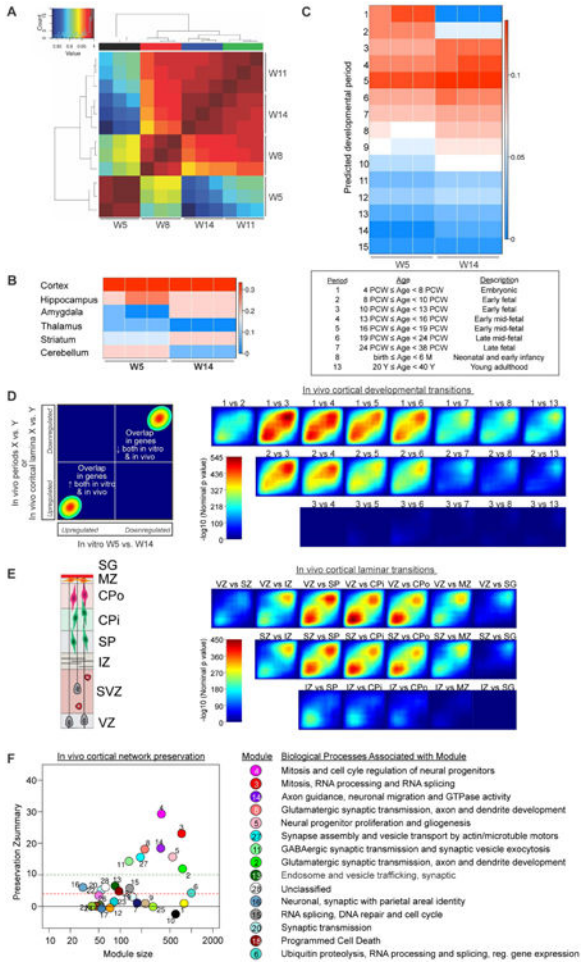

Figure 2. Transcriptomic analyses confirm that cerebral organoids faithfully recapitulate fetal brain development

(**A**) Hierarchical clustering of cerebral organoid gene expression from four time-points (W5, W8, W11, W14), each with three replicates. Heatmap colored according to inter-sample Pearson coefficient from highest (dark red) to lowest (blue) correlation. (**B**) Predicted regional identity of cerebral organoids by CoNTExT analysis. (**C**) Predicted fetal developmental period (defined in table) for W5 and W14 cerebral organoids. (**D-E**) TMAP analysis of developmental (D) and laminar (E) transitions, comparing the progression of W5-W14 organoid to that of indicated pairs of developmental periods. Schematic of laminar organization shown in (**E**). VZ=ventricular zone, SVZ=subventricular zone, IZ=intermediate zone, SP=subplate, CPi=inner cortical plate, CPo=outer cortical plate, MZ=marginal zone, and SG=supragranular layer. Genes upregulated (lower left corner) or downregulated (upper right corner) from in vitro W5 to W14 compared to in vivo transitions. (**F**) WGCNA analysis of developmental processes conserved in organoids versus fetal tissue. Well-preserved modules have preservation Z-score ≥ 4 (dotted red line). See also Table S1.

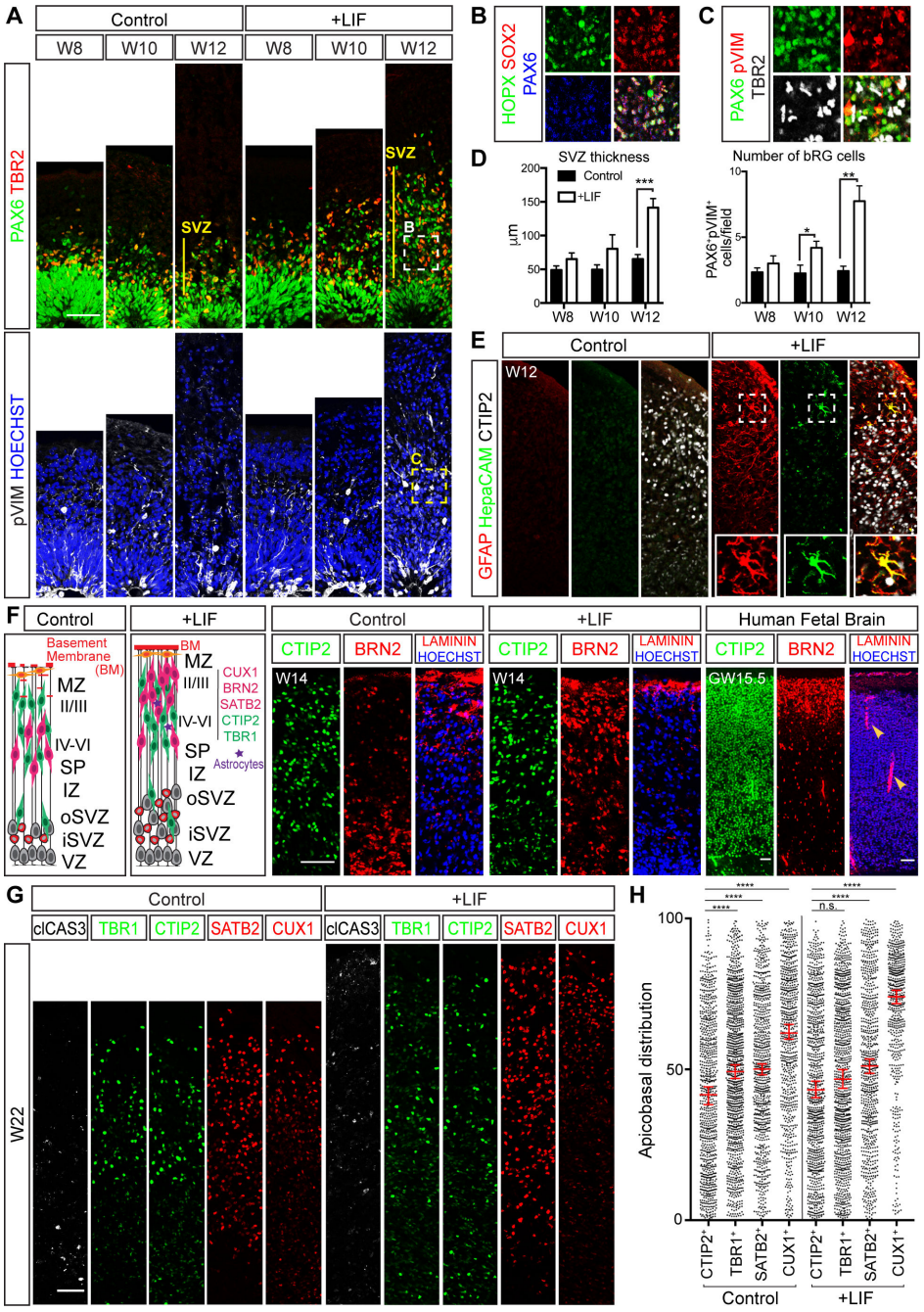

Figure 3. LIF/STAT3 activation increases the formation of bRG cells and stimulates astrogliogenesis

(**A-C**) Cerebral organoids immunostained for general RG (PAX6/SOX2), bRG (HOPX), IP (TBR2), and dividing RG (pVIM) cell markers. (**D**) Thickness of the SVZ in μm and number of bRG. bRG were counted as abventricular PAX6^{+} and pVIM^{+} cells. Data are represented as mean ± SEM. (**E**) Antibody staining for GFAP+/HEPACAM^{+} astrocytes or CTIP2^{+} excitatory neurons in control versus LIF-treated organoids. (**F**) Cerebral organoids and human fetal cortex immunostained for CTIP2^{+} lower layer neurons, BRN2^{+} upper layer neurons, and LAMININ^{+} basement membrane production. Arrowheads denote blood

vessels. (**G**) W22 organoids with or without LIF treatment immunostained for the cell death marker clCAS3, CTIP2$^+$ or TBR1$^+$ lower layer neuronal markers, and SATB2$^+$ or CUX1$^+$ upper layer neuronal markers. (**H**) Relative cortical plate position of CTIP2+, TBR1+, SATB2+, or CUX1$^+$ neurons in W22 organoids with or without LIF. Values represent median ± 95%CI. Total number of neurons counted from 3 independent experiments, Control: CTIP2$^+$ n=,837 TBR1$^+$ n=1088, SATB2$^+$ n=836, CUX1$^+$ n=718; LIF: CTIP2$^+$ n=931, TBR1$^+$ n=1038, SATB2$^+$ n=765, CUX1$^+$ n=546; n.s. no significance, ****$p < 0.0001$, Statistical analysis compares indicated neuronal markers to the CTIP2$^+$ group, Kruskal-Wallis test with Dunn's Correction. All scale bars: 50 μm. See also Figures S4 and S5.

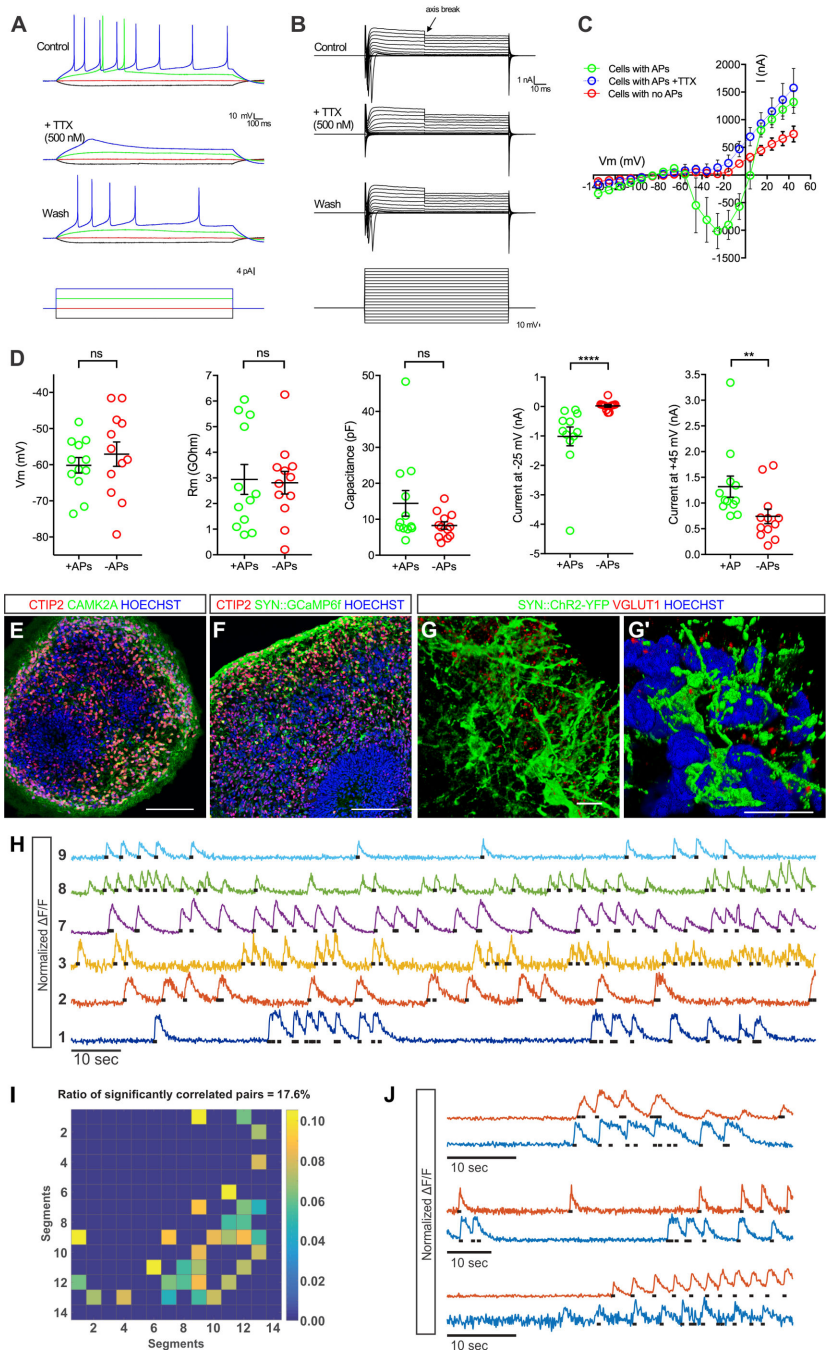

Figure 4. Action potentials and spontaneous network activities in cerebral organoids

W11-W12 organoid slice cultures were prepared for electrophysiological recordings, calcium imaging, and immunostaining. (**A**) Representative TTX-sensitive spike trains upon current stimulation. n=12/24 cells had APs from 3 independent experiments, (**B**) rectified TTX-blocked sodium currents, and (**C**) potassium currents. Data are represented as mean ± SEM. (**D**) Physiological properties of cells with and without APs (membrane potential, membrane resistance, capacitance, peak sodium currents, and peak potassium currents) n=24. Data are represented as mean ± SEM. (**E-F**) Cerebral organoids immunostained for

CTIP2$^+$ excitatory neurons, CaMK2α$^+$ mature neuronal markers, and calcium indicator AAV1-SYN::GCaMP6f (anti-GFP staining). (**G-G′**) 3D reconstruction of axosomatic and axodendritic contacts made between SYN::ChR2-YFP labeled neurons immunostained for the excitatory synaptic marker VGLUT1. (**H**) Normalized GCaMP6f calcium traces from several neurons of an organoid imaged with two-photon microscopy. Black dots indicate action potential time-points extracted from the fast calcium transients (**I**) Matrix of spiking correlation values between all cell pairs in an organoid. Lighter colors indicate higher correlations. Autocorrelation and non-significantly correlated pairs were set to zero. (**J**) Examples of calcium traces from significantly correlated cell pairs. See also Figures S6 and Movie S1. See also Table S4 for statistics. Scale bars: E, F, 100 μm; G, G′, 10 μm.

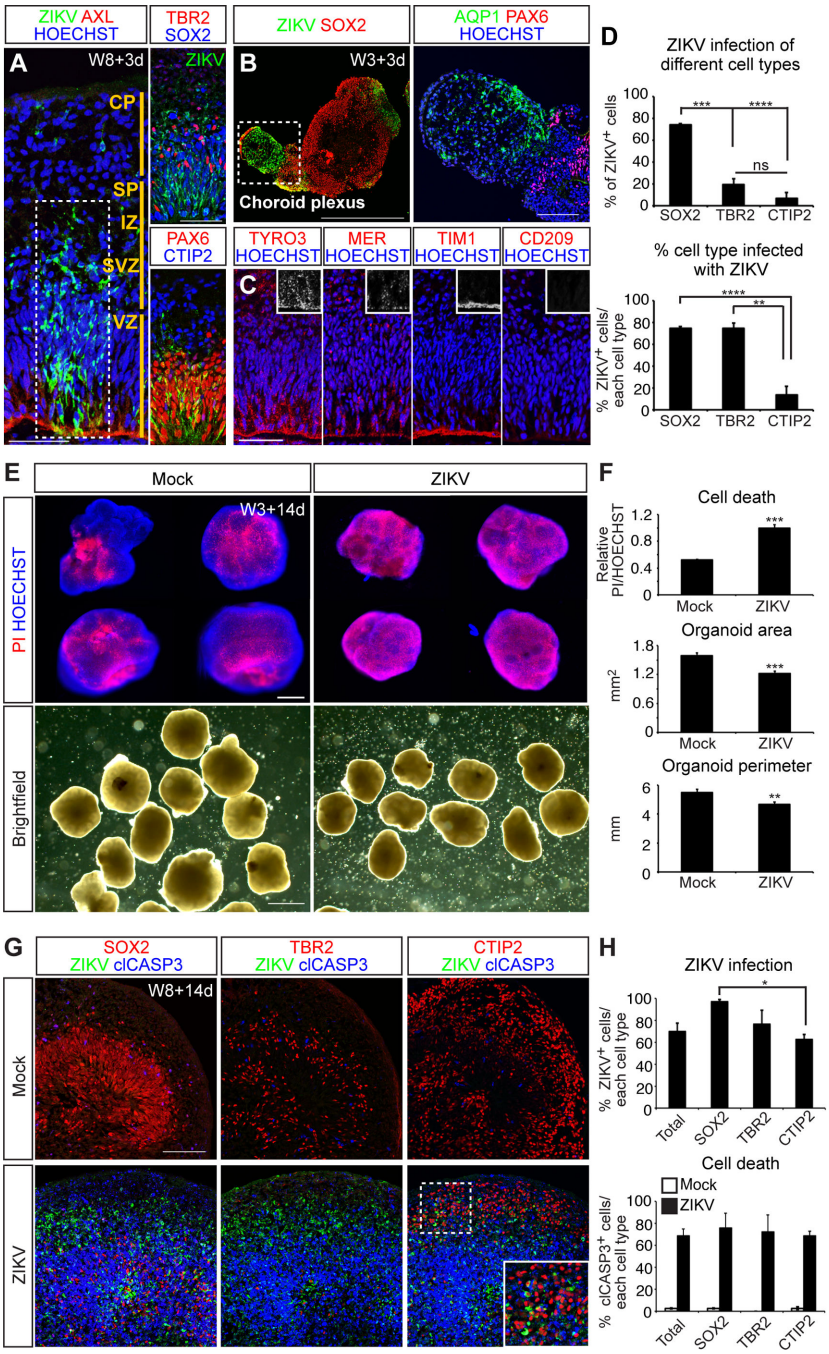

Figure 5. Infection of cerebral organoids with ZIKV leads to widespread progenitor apoptosis and overall growth restriction

(**A-B**) Cerebral organoids immunostained for the ZIKV E protein, candidate ZIKV receptor (AXL), and PAX6+/SOX2$^+$ progenitors, TBR2$^+$ IP, CTIP2$^+$ excitatory neurons, or AQP1$^+$ choroid plexus markers. (**C**) VZ/SVZ regions of W8 cerebral organoids immunostained for the additional ZIKV candidate receptors TYRO3, MER, TIM1, and CD209. (**D**) Top, percentage of all ZIKV$^+$ cells also labeled with indicated markers. Bottom, percentage of each cell type also infected with ZIKV. n=3 independent experiments. (**E**) Cerebral

organoids stained with propidium iodide (PI) to label dead cells and the general nuclear stain. (**F**) Cell death was measured as PI intensity relative to HOECHST, area in mm2, and perimeter in mm. Mock n=23, ZIKV n=26. (**G**) Cerebral organoids collected 14 dpi immunostained for ZIKV, SOX2, TBR2, CTIP2, and clCASP3. (**H**) ZIKV infection was scored as the percentage of each cell type displaying ZIKV envelope staining. Cell death was scored as the percentage of each cell type exhibiting clCASP3 staining. n=3. Data in all charts are represented as mean ± SEM. Scale bars: A, 50 μm; B, 500 μm; E top, 200 μm; E brightfield, 1 mm; G, 100 μm. See also Figure S7.

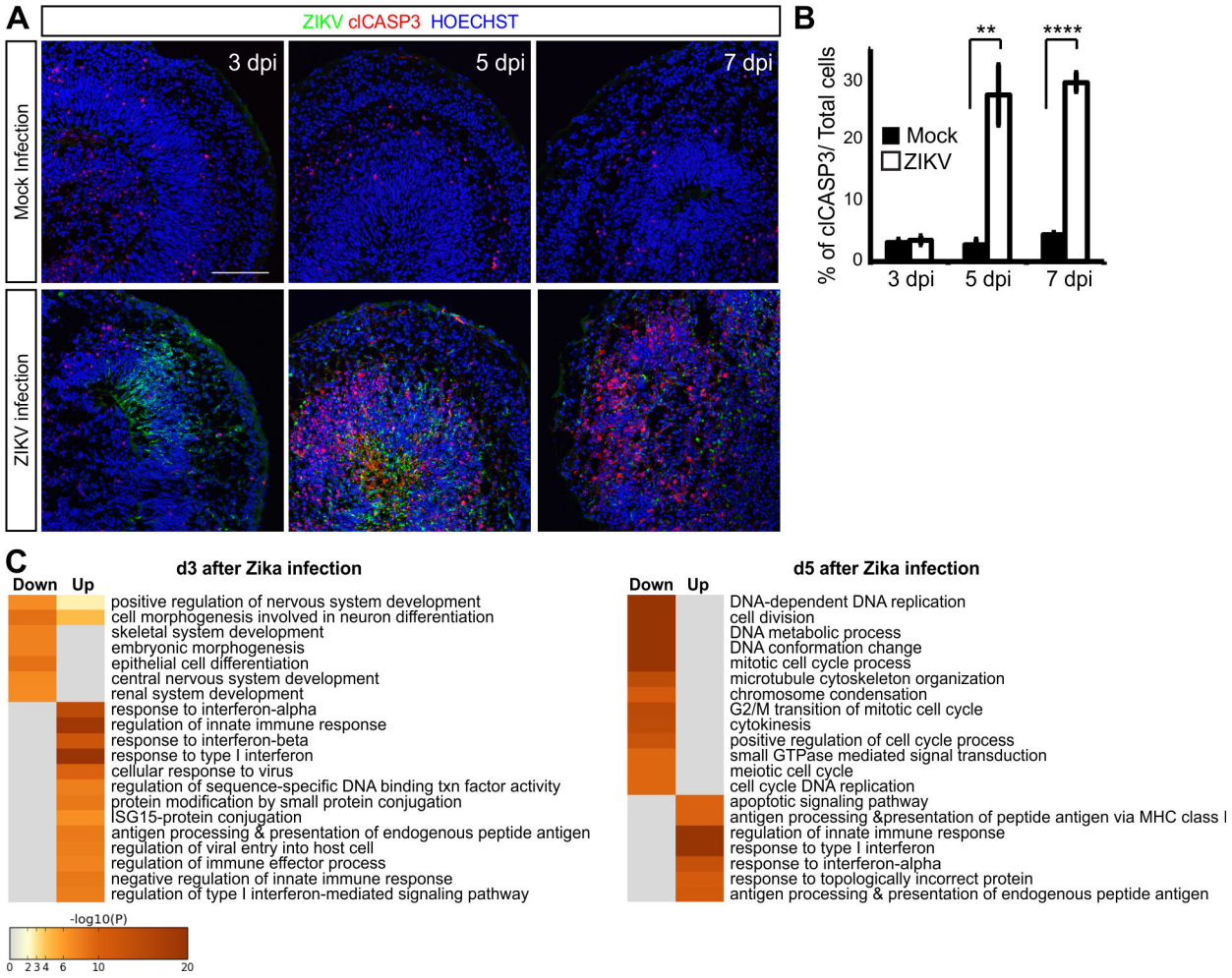

Figure 6. Immune response and programmed cell death in cerebral organoids infected with ZIKV

(**A**) Immunostaining of W8 organoids infected with ZIKV for the indicated number of days. Scale bar: 100 μm. (**B**) Percentage of cells per field positive for clCASP3 out of total cells. n=3. Data are represented as mean ± SEM. (**C**) Gene ontology (GO) annotation of the upregulated and downregulated transcripts in W8 organoids after 3 and 5 dpi with ZIKV compared to mock infected organoids by RNA sequencing. See also the lists of the top 50 upregulated (Table S2) and downregulated genes (Table S3). Cell color represents the –log10 (p-value) for overrepresentation of each GO category within up or downregulated genes. See also Figure S8.

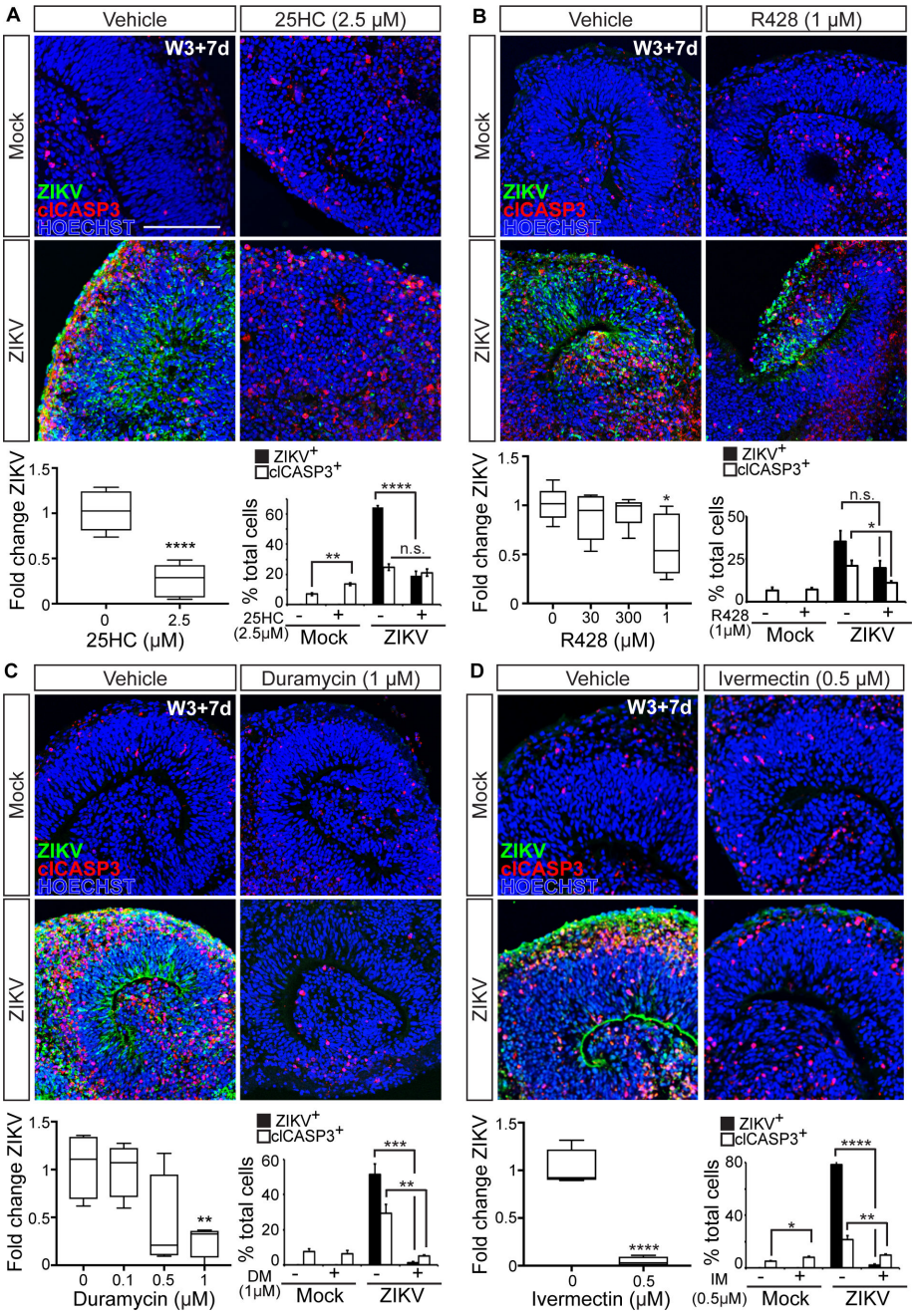

Figure 7. Identification of compounds capable of mitigating the teratogenic effects of ZIKV infection

Cerebral organoids immunostained for ZIKV and cell death marker clCASP3 at 7 dpi in the absence or presence of (**A**) 25HC, (**B**) R428, (**C**) Duramycin, and (**D**) Ivermectin. Scale bar: 100 μm. RT-qPCR analysis of ZIKV expression. Plots represent expression levels normalized to ZIKV-vehicle average. 25HC n=6, R428 n=5, Duramycin n=4, and Ivermectin n=4. Percentage $ZIKV^+$ or $clCASP3^+$ cells out of total cells per field. ZIKV: 25HC: n=6, R428: n=3-4, Duramycin: n=7, and Ivermectin: n=8; clCASP3: 25HC: n=6, R428: n=3-4,

Duramycin: n=3-8, and Ivermectin: n=8-9. Data are represented as mean ± SEM. See also Figure S9 and Table S5 for statistical analysis details.